Masters of Science by Research

Student Name: Ali Ashraf

Student Number: 1011722

Project Supervisor: Prof Andrew Knox

Thesis Title: Locating the Maximum Power Point for Thermoelectric Generators for Constant Heat operation

Contents:

1:INTRODUCTION

In recent years due to increased use of fossil fuels, rising energy costs and environmental concerns such as global warming, there has been a rise in demand for cleaner and more sustainable energy sources [1, 2]. The direct conversion of energy between heat and electricity based on the thermoelectric (TE) effect is an attractive option for achieving this purpose [1-25]. TE energy converters are solid-state devices, do not generate any toxic residuals compared to conventional non-renewable sources of energy and have long term reliability (up to hundred thousand hours of steady state operation) [3, 4]. They can be used in a range of applications demanding different power levels, from wrist watches to large scale waste heat recovery systems *e.g.* in transportation vehicles and in power plants using the Seebeck effect [2][3][5].

ThermoElectric Generators (TEGs) are being used in a multitude of applications such as for vehicular climate control systems [6], waste heat recovery from vehicular exhaust systems [7], and by the aerospace industry for machines operating in hostile and difficult to access environments as sources of electrical power [8]. The application of TEGs is also being evaluated for industrial processes, which involve chemical or mechanical steps and produce waste heat as a by-product [7,8,9]. Thermoelectric generators are also being considered for low power applications such as sensors and for battery charging [10,11].

Conversely these solid-state devices can also be used to convert electrical energy into heat using the Peltier effect. Reversing the polarity of the applied electrical signal to the TE device can change the direction of heat flow across it. TE devices can thus be used for refrigeration applications and as heat pumps [2]. As TE devices do not use any refrigerants or working fluids they may be expected to have negligible direct emission of greenhouse gases [2].

2: Fundamentals of Thermoelectric Effect

The TE effect is characterized by the direct conversion of energy between heat and electricity. Metals and metallic alloys are a known class of materials that exhibit the thermoelectric effect. These are used extensively in thermocouples for temperature measurement and as temperature sensors in control systems [12]. However another class of materials, semiconductors, is also used to construct TE devices. Semiconductors have a Seebeck coefficient in the order of hundreds of microvolts per degree difference in temperature applied across them compared to metals and metallic alloys that have a Seebeck coefficient in the range of tens of microvolts per degree difference in temperature [12].

2a: The Thermoelectric effect

The processes that primarily explain TE energy conversion are the Seebeck effect, the Peltier effect, the Thomson effect and Joule heating. When a temperature gradient is applied across a TE material a voltage is produced which can be used to drive a current through a load resistance in an external circuit. The applied temperature difference causes mobile charge carriers in the material to preferentially diffuse from the hot side to the cold side. The accumulation of charge carriers results in a net charge on the cold side (positive for holes; negative for electrons). This gives rise to an electrostatic potential difference [13]. The chemical potential for diffusion and the electrostatic repulsion due to the build up of charge, reaches equilibrium. This phenomenon is known as the Seebeck effect and is the basis for TE power generation [13]. The device behaves as a thermoelectric generator (TEG) in this case. The generated open circuit voltage can be defined as

$$V_{OC} = S.\Delta T \quad (1)$$

Where V_{OC} *(V)* is the open circuit voltage, S $(\mu V/K)$ is the Seebeck coefficient of the material and ΔT is the temperature difference across the junction (in K or ℃). Fig.1 shows the basic configuration across a single p-n couple that will cause it to behave as a thermoelectric generator.

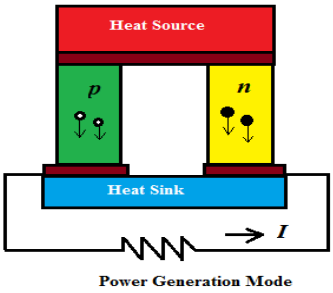

Figure1: Thermoelectric circuit composed of semiconductor materials of different Seebeck coefficients (p-doped and n doped semiconductors) configured as a thermoelectric generator (Seebeck effect) [14]

Conversely, when an electric current is passed through a device, a temperature gradient develops across it. Heat is absorbed on the hot side and rejected to the cold side of the device. The TE device acts a Thermoelectric Cooler (TEC) or Thermoelectric Heat Pump (THP) in this case and the observed phenomenon is known as the Peltier effect. The Peltier heat generated at the junction per unit time can be given by

$$\frac{d\mathbb{Q}}{dt} = (\Pi)\mathrm{I} \tag{2}$$

where $\mathbb{Q}$ is the heat transferred, Π (measured in *W/A* or in *V*) is the Peltier coefficient for the material and *I(A)* is the current through the junction. Reversing the direction of applied current through the device reverses the temperature gradient cross it [13]. Fig.2 below shows the configuration across a p-n couple to produce the Peltier effect.

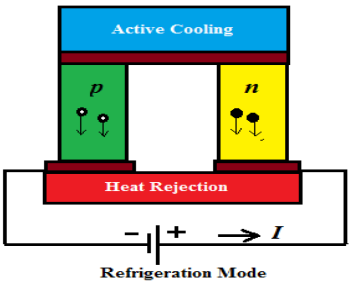

Figure2: Thermoelectric circuit composed of semiconductor materials of different Seebeck coefficients (p-doped and n doped semiconductors) configured as a thermoelectric cooler (Peltier effect) [14]

The Thomson effect relates the reversible heat q generated because of passage of current I through a semiconductor across which is a temperature differenceΔT.

$$\mathbb{Q} = \tau . I . \Delta T \tag{3}$$

Equation (3) describes the Thomson effect for small temperature differences [1]. $\mathbb{Q}$ is the heat transferred due to the Thompson effect, τ (*V/K*) is Thompson coefficient of the material, *I(A)* is the applied current and ΔT is the temperature difference. The Thomson effect is not of primary importance in TE devices as it is small enough to be

ignored for most analyses. However, it should not be neglected when carrying out detailed calculations [13].

The three effects are interdependent and explain the collective term, the Thermoelectric Effect. The Kelvin relations summarize their interdependencies

1. $\Pi = ST_j$
2. $\tau = \frac{dS}{dt} T_{avg}$

Where T_j is the junction temperature and T_{avg} is the average material temperature. These relations hold true for all materials [13].

Joule heating, also known as ohmic heating or resistive heating, is a process by which heat is generated when an electric current is passed through a conductor. Unlike the Peltier effect, Joule heating is independent of the direction of the applied current. Due to the internal electrical resistance of the TE material, heat is generated inside the module itself when an electric current is passed through it [13][14]. When connected to a load resistance, all aforementioned phenomenon influence TE performance of a device to a greater or lesser extent.

TE modules consist of multiple pairs of cuboid shaped pellets (thermo-elements) of semiconducting material connected electrically in series and thermally in parallel. Figure 3 shows a typical TE module for generating power. Different materials are used to construct these thermo-elements, where the performance of each material is optimized for a specific temperature range. Bismuth and its alloys with antimony, tellurium and selenium are referred to as low temperature materials for constructing TE devices and can be used for temperatures up to 450K-500K [13]. Materials such as lead telluride are used to construct modules that can be used up to temperatures as high as 850K [15]. For even higher temperatures (up to 1300K) TE materials are constructed using silicon germanium alloys and materials such as skutterudites and clathrates [13] [7]. TEG and TEC (or THP) modules are similar to one another in terms of their basic construction. Applying a current to a TE device will cause it to behave as a TEC (or THP) and applying a temperature gradient to it will cause to behave as a TEG. However TE devices are optimized for each of these processes and hence modules used for refrigerating have a different geometry and are made from different materials compared to modules used for power generation. TECs are optimized to work closer to room temperatures as usually found in cooling applications and TEGs on the other hand are made to function at higher temperatures. The thermo-element size is larger in TEGs generally as larger element size means more heat flow hence more power. TEC modules on the other hand can have features

such as thicker leads for more current flow to increase the heat pumping process. Therefore, despite having very similar basic construction subtle differences exist between TEGs and TECs (or THPs).

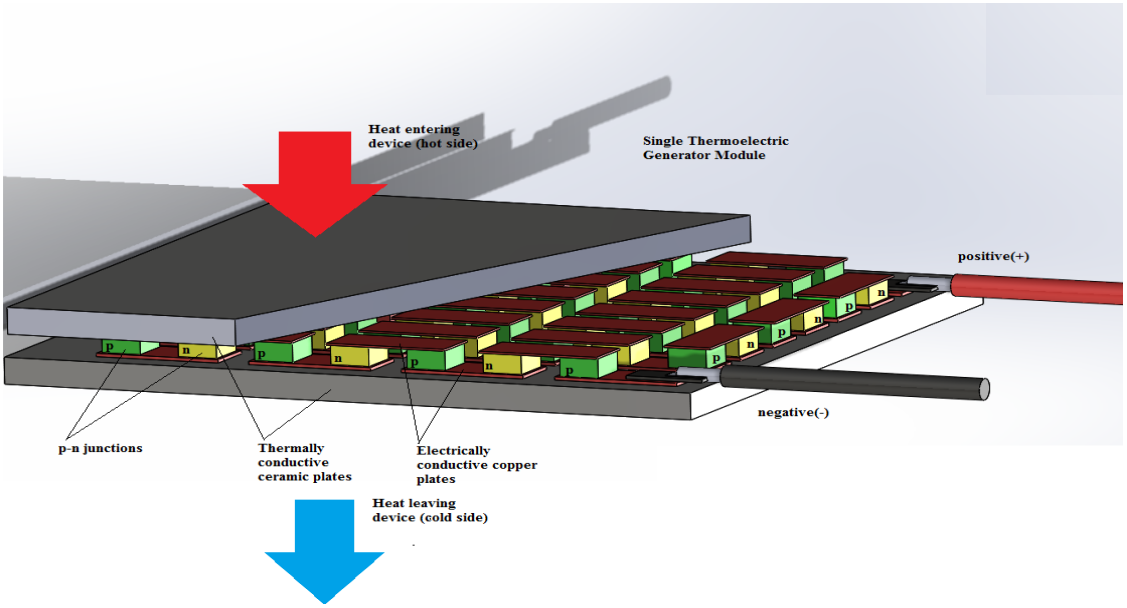

Figure3: Cut away section of a TE generator

2b: <u>Efficiency of thermoelectric materials and areas of improvement</u>

The maximum efficiency of a TE converter greatly depends on the temperature difference across it. This is because like all heat engines, a TE converter cannot have efficiency greater than that of the Carnot cycle [14].

The figure of merit ZT is parameter often quoted to judge a material's feasibility for being used in a TE module. It is a dimensionless quantity. Most commercially available modules have a Figure of Merit not greater than 1 [13]. ZT is defined as

$$ZT = \frac{S^2\sigma}{k} \qquad (4)$$

Where ZT is the figure of merit, S is the Seebeck coefficient, σ (S/m) is the electrical conductivity of the material and k $(W/m.K)$ is the thermal conductivity of the material. Looking at Eq.4 one can conclude that materials with a high figure of merit will possess the following characteristics.

1. Low Thermal conductivity (to maintain temperature gradient across module)
2. Low internal resistance (high Electrical Conductivity)
3. High Seebeck Coefficient

According to Snyder [14] to calculate the exact efficiency of a thermoelectric material is complex but by making the assumptions that the Seebeck coefficient, the thermal conductivity of the material and the electrical conductivity of the material are all

independent of temperature leads to a simple expression for the efficiency of a thermoelectric material in terms of ZT

$$\eta = \frac{\sqrt{1+ZT}-1}{\left(\sqrt{1+ZT}+\left(\frac{T_c}{T_h}\right)\right)} \quad (5)$$

Where η is the efficiency of the material, *ZT* is the Figure of Merit, and T_c and T_h are the cold and hot junction temperatures across the TE module respectively. It should be noted, however, that *ZT* is not the only parameter to judge how 'good' a TE material and in effect a TE module is. Other factors such as the application and temperature the TE material is being used at, the length of the pellets and the geometry of the module all are indicators of how well the module may perform.

To date, existing materials used to manufacture TE devices do not allow for a very high efficiency ($\backsim$ 5%) [10,16]. However, we can better incorporate TE devices in energy recovery systems by improving the overall system efficiency to harness maximum advantage from available modules.

3: Literature Review

There has been substantial work done for characterizing TE material performance. However, to date no standardized method exists for assessing TE module performance and characterization of TE module parameters such as the open circuit voltage, the Seebeck coefficient of the module, the short circuit current, the power output of the device and the overall device efficiency [5,18,19; 20-22]. These parameters are necessary for design engineers to produce systems that make optimal use of available modules. Figure 4 shows the minimum parts required for generating power from TE modules, which is very similar in all test systems; the hot side heat exchanger, the cold side heat exchanger, system insulation and of course the generator itself (TEG).

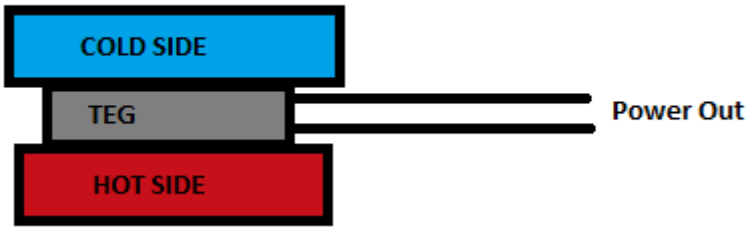

Figure4: Arrangement for testing a TEG (insulation layer is omitted for clarity)

IIIa: Various Test systems used to characterize TEG performance

Karabetoglu Sisman *et.al* [9] have developed a test system to characterize the thermoelectric performance of a commercially available bismuth telluride (Bi_2Te_3) based TEGs at low temperatures (up to 500*K*). A TEG is sandwiched between two copper plates that act as hot and cold sides respectively. An electric heater is used to provide thermal energy to the hot side and liquefied nitrogen is used as a coolant on the cold side. *K* type[1] thermocouples are used to make measurements of temperatures. Standard current and voltage sensors are used to measure the current and voltage and the heat flux through the TE material is calculated analytically. Extruded Polystyrene (XPS) foam (a form of rigid insulation used in buildings) insulator surrounds the TE module to minimize heat losses to environment. Parameters such as maximum power the TEG can produce and the average Seebeck coefficient of the module were determined.

A similar system was developed by Dalola Ferrari *et.al* [10] for characterizing TE module performance for powering autonomous sensors. Two thermo-stating circuits

[1] K type thermocouples are thermocouples made from alloys chromel and alumel. These are one of the most commonly used thermocouples due to their large measurement range (-200℃ to +1350℃). Tolerance class 1 K type thermocouples have a tolerance of±1.5℃.

using auxiliary thermoelectric modules are used to impose desired hot and cold side temperatures on each side of the TEG. The thermo-stating circuits have negative temperature coefficient (NTC) thermistors to measure the temperature on each side of the TEG and a potentiometer to vary the desired temperature value. The system was used to assess the output performance of the TEG and measure its open circuit voltage for different temperature gradients and different load conditions.

The test system developed by Havrylyuk and Anatychuk [15] measures TEG module parameters in the temperature range of +30℃ to +600℃. It uses heat meters to measure the heat flux through the module directly. The hot side heat exchanger in the system is a copper block powered by a resistive heater. The cold side heat exchanger is a copper block, which is cooled by flowing water through it. The fixture uses a manual compression unit to apply a uniform clamping force across the TEG (compression force of up to 1800N can be applied). The clamping force ensures good thermal contact between the TEG, hot side and cold side surfaces. The fixture can accommodate TEGs from sizes of 10mm x 10mm to 100mm x 100mm. The hot side temperature can be varied from +50℃ *to* +600℃ and the cold side temperature can be varied from +30℃ to + 90℃. Errors reported by the authors include measurement of heat flux through module and measurement of TEG surface temperature (maximum of $\pm$0.5℃).

Rauscher, Sano *et.al* [16] developed a very similar system to [15] to test the efficiency of a TEG using absolute measurement of the heat flow. The additional feature in their apparatus was a guard heater placed on the hot side heat exchanger to compensate heat losses in the system and more accurately measure the heat flux in to the TE module compared to [15] in which there was no compensation of heat losses to ambient.

Other test systems developed include a test system that measures the efficiency of the thermoelectric modules operating in a temperature difference of up to 550*K* by Takawaza, Obara *et.al* [11] and by Rosado-Sandoz and Stevens [23] which does experimental characterization of thermoelectric modules and compares them with theoretical models for power Generation.
Han, Kim *et.al* [16] use a cooling fan on the cold side heat exchanger to maintain a temperature gradient and aluminum blocks instead of copper blocks as heat

exchangers. Aluminum has a lower melting point than copper (aluminum: 660℃; copper: 1085℃). Consequently higher operating temperatures cannot be tested. Han, Kim *et.al* [24] using their test apparatus also analyze the relationship between individual pellet heights in the module (n-p junctions that make up the module) and the performance of the TEG. They concluded that, as pellet length decreases, the voltage, current and output power of TEG increase because the internal resistance of the TEG decreases.

Carmo, Antunes *et.al* [25] designed an experiment where the TEG was placed between two copper blocks acting as heat exchangers, with the hot side placed on a temperature controlled hot plate and the cold side being cooled by a fan (forced air convection). Temperature measurements on each face of the TEG were recorded using thermistors. They have used the setup to characterize the electrical load dependence behavior of TEGs.

Lab-view was the most commonly used control software among the above discussed [9,10,11,15,16,23,25] test systems to implement hot side and cooling side temperatures and to record measurements.

Discussed in this section so far are a few examples of test systems designed by researchers to examine TE module parameters. The examined parameters include output open circuit voltage, current through the device, effect of module geometry and factors such as pellet length on the overall efficiency of the module, module behavior for various temperature differences and for various operating temperatures and the Seebeck Effect.

3b: Constant Heat vs. Constant Temperature

Assuming the hot and cold side temperatures are constant and therefore there is a constant temperature difference (ΔT) across the TEG module, the TEG can be electrically modeled as a voltage source in series with a constant internal resistance [26]. If this is the case then according to the maximum power transfer theorem, the maximum power point of the TEG lies at exactly half the open circuit voltage (V_{oc}) of the TEG. At this point the impedance of the TEG is matched by the load impedance and enables extraction of maximum electrical power from the TEG [26].

The prevalent method of TEG characterization is by applying a constant ΔT across a TEG module and extracting parameters such as voltage, current and the electrical output power from the TEG and is referred to as 'constant temperature characterization'. Fig.5 shows the commonly produced electrical characterization graph for TEGs.

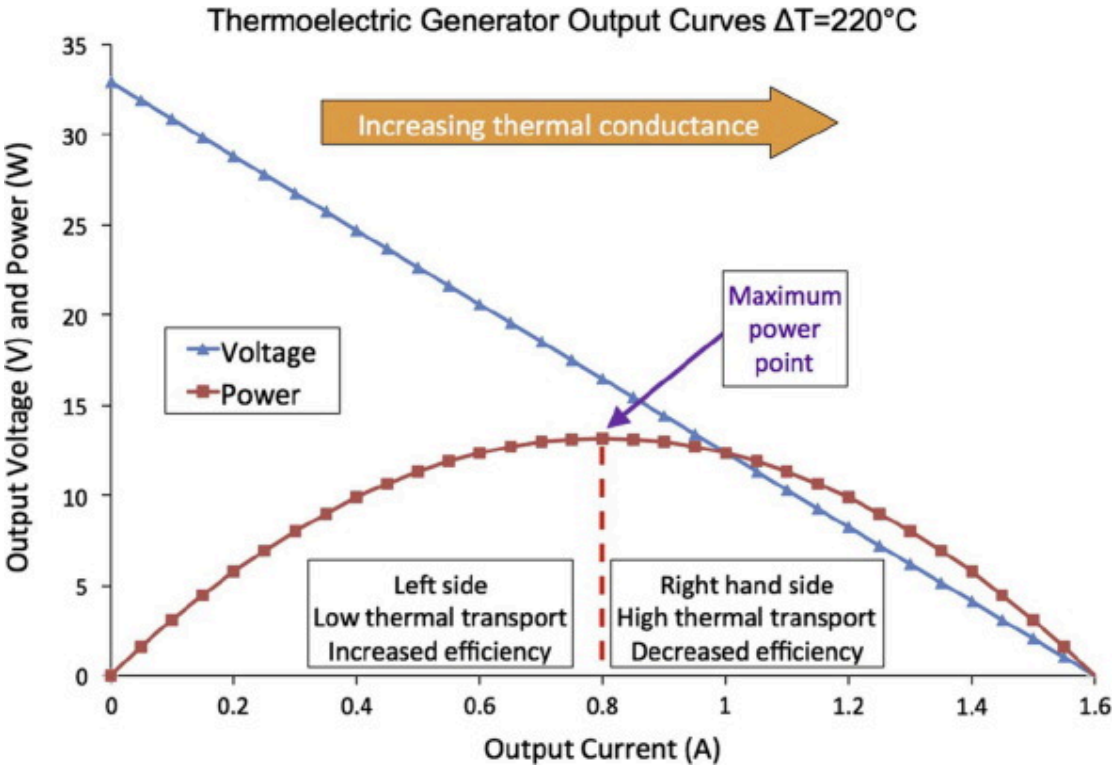

Figure5: Constant temperature characterization of a TEG from European Thermodynamics [26]

The internal resistance of the TEG (R_{int}) is determined from the slope of the *V-I* curve obtained from this characterization. As the load resistance across the TEG changes, moving from open circuit to short circuit conditions, the effective thermal conductivity of the TEG increases [27]. An increase in thermal conductivity means

more heat flux flows through the TEG and the temperature difference across the TEG would decrease. Therefore to maintain a constant temperature difference across the TEG, the heat flux has to be constantly adjusted [28].

In most real applications, the case is reversed. In most waste recovery systems, there is a fixed amount of thermal energy available and the temperature difference across the TEG varies as the load resistance across it changes. To maximize the power produced by TEGs under different thermal conditions at any time Maximum Power Point (MPP) converters are used. Commonly used algorithms such as the fractional open circuit algorithm [29] and the hill climbing algorithm [30,31], both set the operating load at half the open circuit voltage, which is MPP operating condition for constant temperature systems. Thermal and electrical properties of TEGs, such as the thermal conductivity, electrical resistivity, and Seebeck coefficient are all temperature dependent [32]. Li *et.al* [32] suggest that the thermal and electrical properties of thermoelectric pellets play a pivotal role in module performance *i.e.* output electrical power produced by the TEG. Therefore it would be unsuitable to use constant temperature operation techniques to determine the maximum power point for constant heat systems.

A prime example of this is the automotive exhaust gas recovery systems. Kumar *et.al* [33] has stated that the electrical power out from the TEG strongly varies with the inlet exhaust temperature. They concluded that varying inlet temperatures can adversely affect the waste heat recovery system if proper conditioning of output power is not carried out. [33]. Niu *et.al* [34] observed similar results to [33] for their experimental study on low temperature waste heat thermoelectric generator systems. Commercially available thermoelectric generators were coupled with parallel plate heat exchangers. It was found that the hot fluid inlet temperature and the fluid flow rate significantly affect the maximum power output and conversion efficiency of the TEG.

It was noted by Min [28] that the voltage, current and power output values for TEGs operating in constant heat systems was lower than that for TEGs operating in constant temperature systems. This is because, as explained on pg12, the temperature difference across the TEG reduces for constant heat systems as the load resistance decreases. Mayer and Ram [35] arrived at similar conclusions, stating that the

optimum current for MPP operation is lower for a varying temperature gradient across the TEG (as in constant heat systems) than that for constant temperature systems.

Youn *et.al* [36] state that for practical waste heat recovery systems, the impedance-matched condition is not identical to the maximum power output condition. Gomez *et.al* [37] compliment this analysis. They state that contrary to previously reported constant temperature analyses in the literature where maximum power occurs for impedance matching conditions and maximum efficiency occurs at $R_L = R_i\sqrt{1 + ZT_m}$ (where R_L is the load resistance, R_i is the internal resistance of the TEG module, Z is the figure of merit and T_m is the average module temperature), for systems where the effect of electrical current on the temperature of the TEG module are taken into consideration the optimum value (MPP) for the resistance ratio is much higher than that for constant temperature models.

Montecucco *et.al* [29] have attempted to characterize TEG electrical performance for a constant heat system. They have drawn similar conclusions to [28][35][36]. The characterization is done in a MATLAB simulation, using minimal experimental data. The bulk of research carried out for this report has focused on preparing a constant heat experimental setup to characterize the electrical performance of thermoelectric generators for constant heat conditions.
The research has been divided in to the following subtopics

1. Prepare a constant heat test system
2. Investigate the true position of the maximum power point (MPP) of TEGs operating under constant heat conditions

To summarize this section, for most practical thermoelectric energy recovery systems, there is limited thermal energy available and constant temperature characterization of thermoelectric modules is not the correct way of determining their performance in real world waste heat recovery systems. Also electrical impedance matching to achieve MPP for TEGs operating under constant temperature conditions will not achieve the true MPP. According to the bulk of the literature discussed in this section, for constant temperature conditions, the MPP and maximum efficiency point are different. This is because during constant temperature conditions the hot side heat exchanger and cold side heat exchanger temperatures are held constant, varying the thermal input to the system according

to how the Peltier effect modifies the thermal conductivity of the TEG. In constant heat system, the contrary happens. There is limited thermal input power available to the TEG and the temperature across the TEG varies depending on the electrical load across it, *i.e.,* in accordance with the Peltier effect due to the current flow. Since the available thermal input power is fixed, the MPP and maximum efficiency lie at the same point.

As TEGs when integrated in a system and operating *under constant heat conditions* generally do not have a MPP at $\frac{V_{oc}}{2}$ (impedance matched conditions), it is useful to know at what fraction of the instantaneous open circuit voltage of the TEG it will produce the most output electrical power for a given thermal input.

For constant heat operation the true MPP lies to the left of constant temperature power curve shown in Fig.5 pg.12, as established by [29,33,35,36,37] *i.e.* it is greater than $\frac{V_{oc}}{2}$.

The load voltage of the TEG, V_{load}, can be expressed as a fraction of the instantaneous open circuit voltage of the TEG, V_{oc_inst}, as

$$\beta = \frac{V_{load}}{V_{oc\_inst}} \tag{6}$$

Where β is a dimensionless number, V_{oc_inst} is the open circuit voltage obtained immediately after the TEG is disconnected from the load. This differs from the open circuit voltage that would be established if the TEG was disconnected from the load and left to reach thermal equilibrium. The value of β that leads to maximum power from the TEG is to be investigated ($\beta_{\max}$).

4: EXPERIMENTAL SETUP

4a: Initial Experimental Setup

Initial investigation of the true maximum power point was carried out using a basic experimental setup provided by Thermoelectric Conversion Systems. Fig.6 shows the block diagram for the test system used.

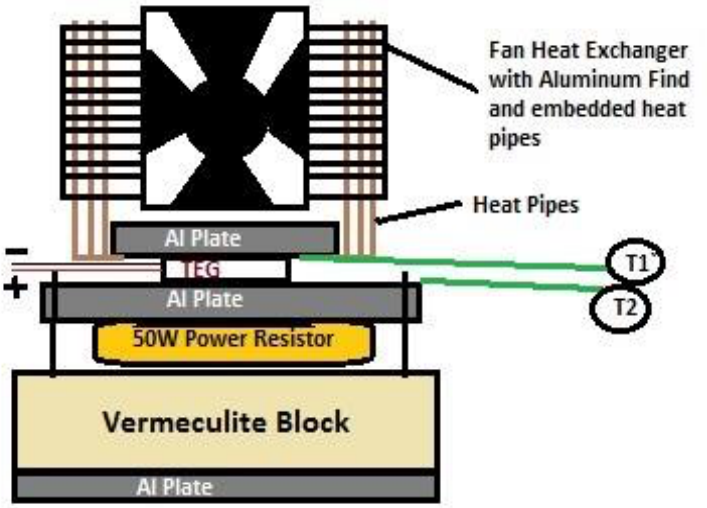

Figure6: Test system for initial investigation of the true position of the maximum power point for TEGs. T1 is a thermistor and T2 is a K-type thermocouple.

This initial test system has a fan heat exchanger for the cold side heat exchanger of the TEG. The fan-cooled heat exchanger is attached to aluminum fins with copper heat pipes embedded in them. One end of the copper heat pipes is attached to an aluminum plate. The hot side heat exchanger also uses an aluminum plate with a 50W power resistor screwed on to its base. Thermal grease is used between the power resistor base and the aluminum plate to aid heat transfer between the two. A GM200-127-10-12 30x30 mm bismuth telluride TEG is placed between the two aluminum plates, with thermal grease between the plates and the TEG to facilitate heat transfer. The TEG is clamped between the two plates using screws bolted through from each aluminum plate in to the vermiculite block. A thermistor is bolted on the face of cold side aluminum plate to measure the cold side TEG face temperature. A K-type thermocouple is placed on the hot side aluminum plate to measure the hot side face TEG temperature. The stack is then surrounded by fiberglass to reduce the thermal losses to ambient.

The TEG is connected to an Electronic Load (Agilent N3300A). The electronic load is used to read the TEG V_{oc_inst} and then update the value of V_{load} accordingly. The thermocouple and thermistor are connected to a data logger (Agilent N32702A). The power resistor is connected to a power supply unit (Agilent N5720A PSU). The electronic load, the data logger and the power supply unit are connected to a laptop computer for partial control and to record required data.

A constant heat experiment was run for 3 different input electrical powers to the heaters, 45W, 33W and 23W. This initial experiment was intended to provide evidence that for TEGs operating in a constant heat system the position of the true MPP is greater than $\frac{V_{oc}}{2}$.

For this initial testing, it was assumed that the electrical energy to the power resistor is the thermal input energy to the TEG and the thermal losses to ambient from the power resistor are negligible. Therefore all the thermal energy flows through the TEG *i.e.* the system has one-dimensional heat flow. For each thermal input power β is set to be 0.5 at the start of the experiment. V_{oc_inst} is recorded and V_{load} is updated every 2s according to the value of β . The system is allowed to reach thermal equilibrium (*i.e.* when the hot side aluminum plate temperature is constant within $\pm 0.2℃$ for more than 1800s) and the thermal steady values of V_{load}, I_{load} and TEG hot and cold side temperatures are recorded. The value of β was then incremented by 0.1, and the whole process repeated till the electrical power output from the TEG starts to decrease. Fig.7a demonstrates the measurement process in a flow chart. Fig.7b below show the electrical power output from the TEG for various values of β for the different input thermal powers.

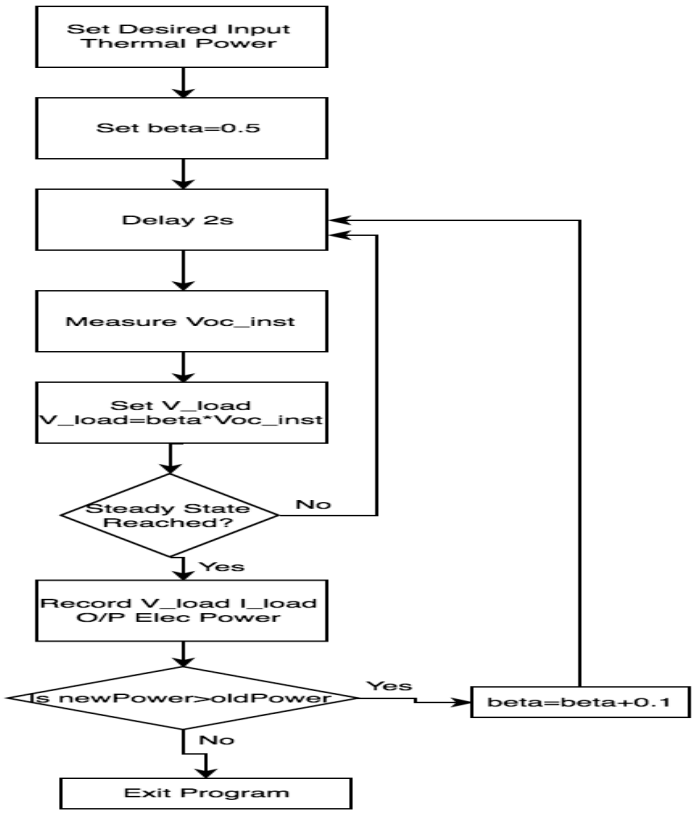

Figure7a: Flow chart for program to determine the position of MPP

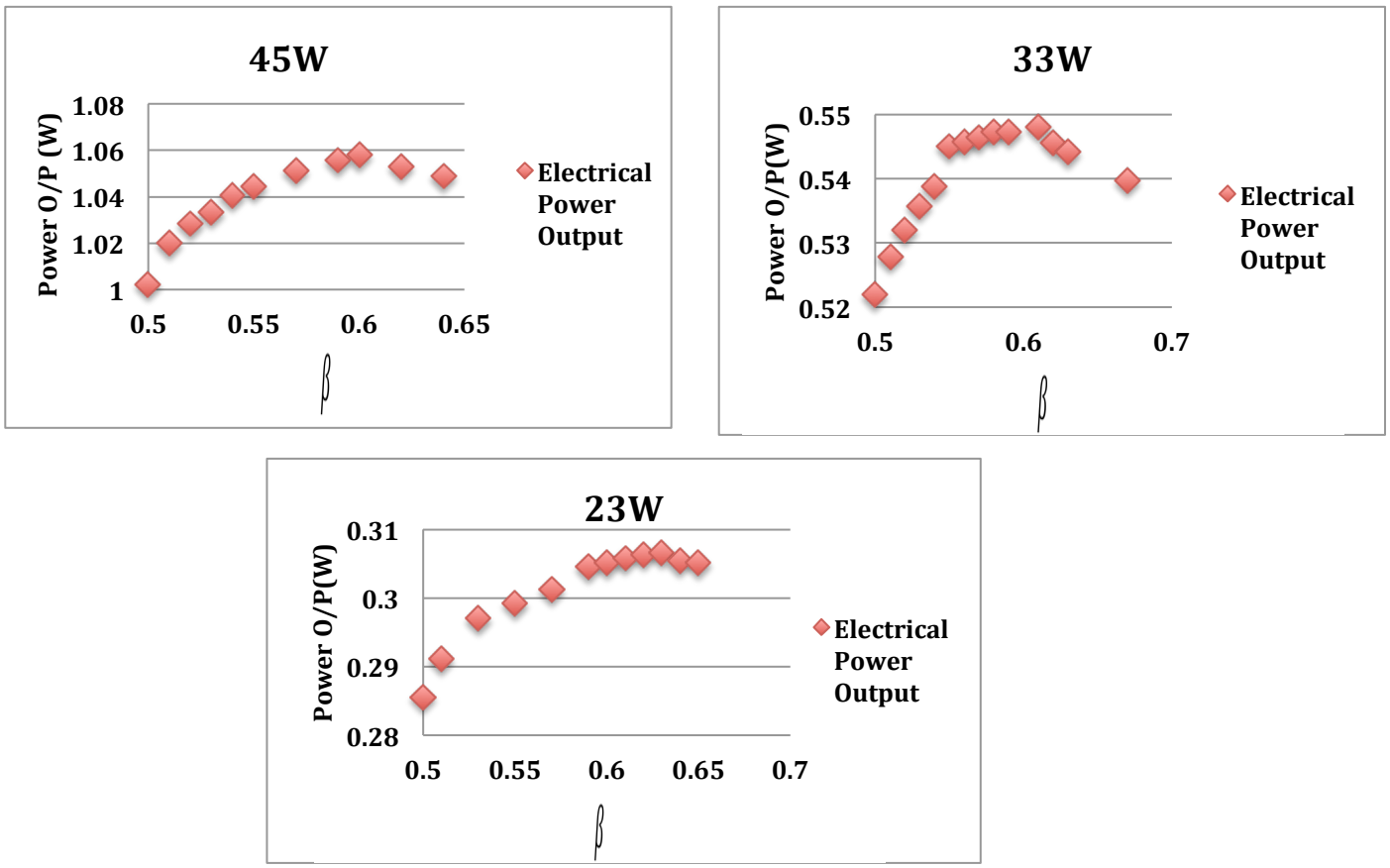

Figure7b: Electrical Power output from GM200-127-10-12 30x30mm TEG for different values for input thermal power with respect to β

From Fig.7b it can be seen that there is an increase in the output electrical power of the TEG as the value of β is increased and after a certain value of β is reached the output electrical power starts to decrease. However, there are several parameters in this initial experiment that need to be standardized before the results can be fully analyzed. These are:

1. Thermal Losses to ambient
2. System Insulation
3. Clamping force on the TEG
4. Range of input thermal powers available
5. Better overall temperature measurement accuracy
6. Temperature control on the cold and hot side heat exchangers

To perform an accurate analysis of the true position of the MPP the above mentioned parameters need to be adjusted in the following way:

1. Even though fiberglass has a very low thermal conductivity ($0.4W/mK$), the assumption that the fiberglass insulation makes thermal losses negligible was not correct. The main source of thermal losses to ambient is the hot side heat exchanger and as the temperature of it increases, the losses to ambient increase as well. To know exactly know the heat flux entering the TEG from the hot side heat exchanger, the heat losses to ambient had to be characterized in the second iteration of this experiment.
2. Using fiberglass for insulation, it was nearly impossible to attain the same placement and packing density of insulation each time it was removed when the system was unloaded. Therefore for a particular steady state temperature of the hot side heat exchanger, the thermal power lost to ambient would be different each time the system has to be unloaded. To ensure thermal losses to ambient remain constant, a more rigid form of insulation was required. Fiberglass placement makes a slight difference to the overall thermal resistance of the system to ambient but it is significant enough to have an impact on the results hence it is considered.
3. For a constant heat test, as the temperature varies, the heat exchangers contract and expand and therefore the clamping force with which the TEG is held between the two heat exchangers changes. Constant clamping force is needed

to remove variability in the thermal conductance between the heat exchangers and the TEG surface to allow for test repeatability.

4. This experimental setup can only be used to test very low input thermal powers (maximum 50W). Also different sizes of TEGs cannot be tested on this system.
5. The cold side heat exchanger temperature is measured using a thermistor, which has a precision of ± 1℃. Better precision is can be attained using thermocouples, which have been calibrated using a mercury thermometer. Thermocouples have an absolute precision of ± 1℃. A mercury thermometer can, which has an absolute precision of ±0.1℃, can be used to calibrate these thermocouples to ± 0.1℃. Hence better over accuracy can be achieved.
6. The temperature on the heat exchangers cannot be controlled in this system due to lack of temperature feedback.

4b: Final Experimental Setup

To perform a more accurate constant heat characterization of thermoelectric generators, another test system from Thermoelectric Conversion Systems (TCS) was used. It is modified slightly for the needs of the investigation as will be discussed in this section. Fig.8 shows a block diagram for the test system.

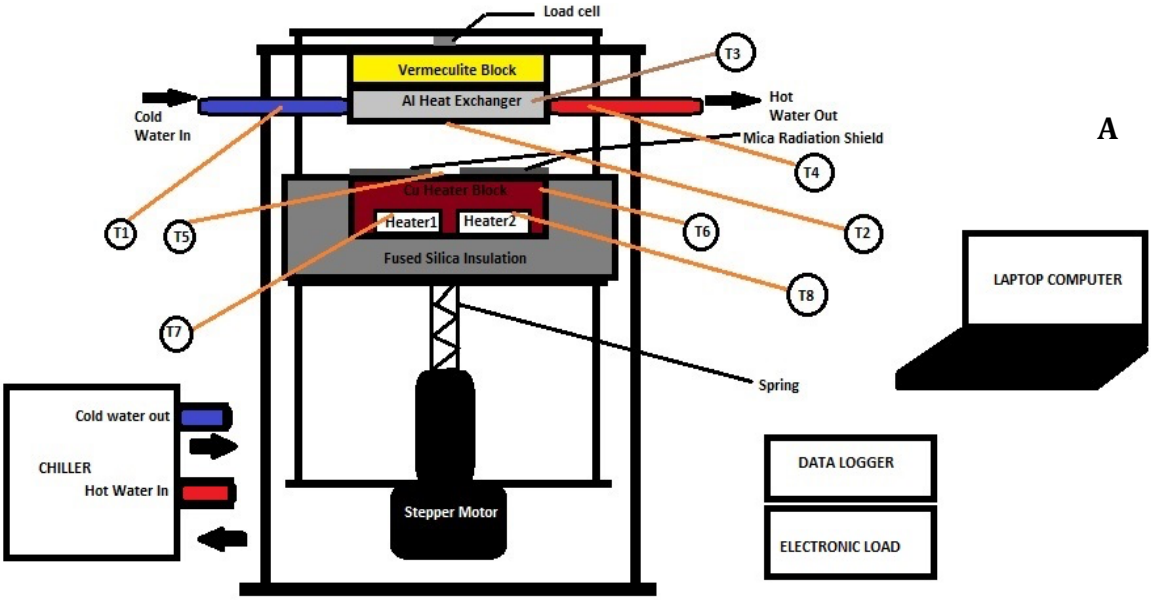

A

B

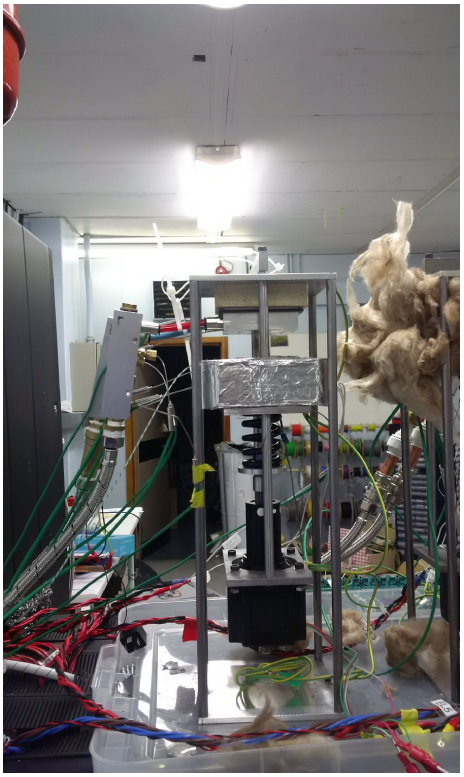

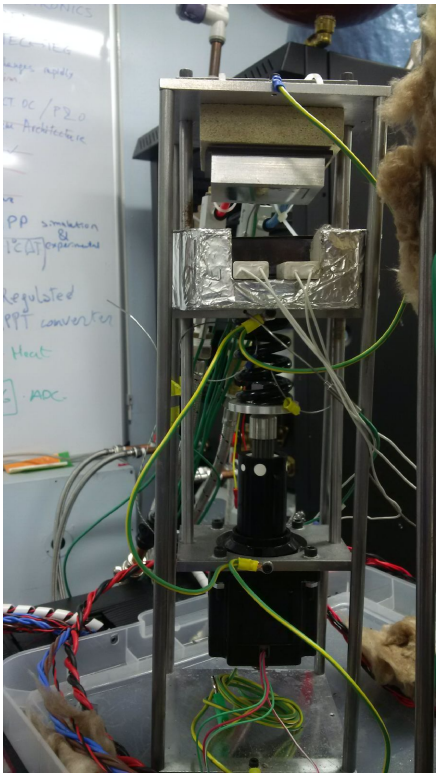

C

Figure8: Test System used to investigate the position of maximum power point. A: Block Diagram for the test system (T1-T8 represent position of thermocouples). B: Side view of the Test System. C: Front of the Test System.

4b.1: Heat Exchangers

The test system uses a $75\times75\times25.4mm$ water-cooled aluminum heat exchanger. The aluminum heat exchanger is connected to a 1kW chiller, which can be used to maintain a desired water temperature with a ±0.1℃ precision. The aluminum heat exchanger acts as a cold side heat exchanger. A vermiculite insulation block thermally decouples the cold side heat exchanger from the hot side heat exchanger as shown in Fig8A. This prevents any thermal shorts from happening in the system. The water temperature is set to 24℃, close to ambient temperature to avoid condensation.

A $75\times75\times25.4mm$ copper block, with two silicon nitride cartridge heaters embedded in it is used as the hot side heat exchanger. Each cartridge heater is rated for 500W of power and therefore the heater block can deliver a total of 1kW of thermal power. The copper block size is chosen to accommodate the largest possible available thermoelectric modules ($62\times62mm$). The Cu block is surrounded by $25.4mm$ thick fumed silica insulation, covered by aluminum foil tape, on each side except the top face. The aluminum foil reduces thermal power lost to ambient through radiation. Fumed silica insulation is used because of its very low thermal conductivity ($0.02W/mK$ at 200℃), as shown in Fig.9.

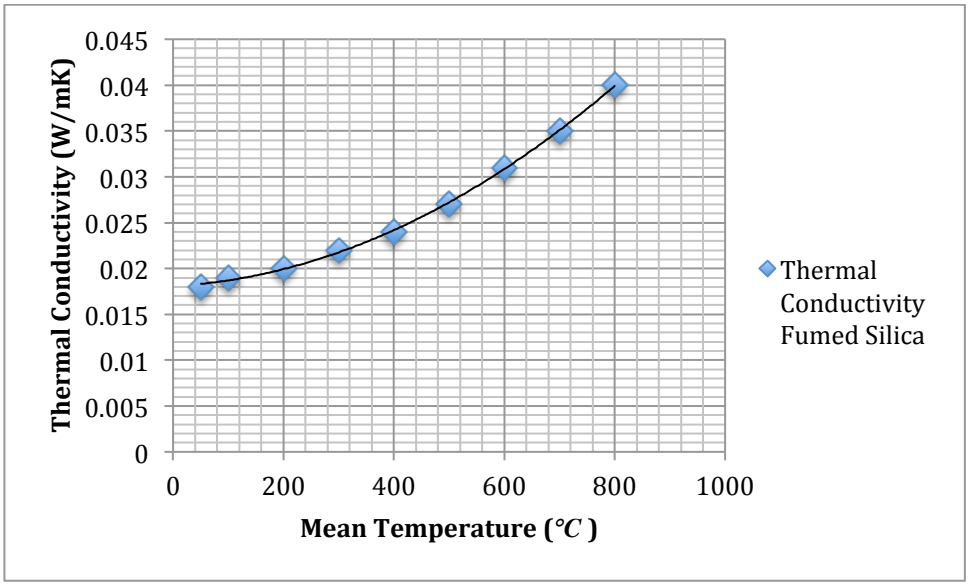

Figure9: Thermal conductivity of fumed silica insulation board as a function of mean temperature as specified by manufacturer

The original test setup used fiberglass to help insulate the system. Fibre glass not only has a higher thermal conductivity ($K = 0.04W/mK$), it is also hard to ensure the same packing density and insulation placement is achieved each time it is removed and put back in when the system is unloaded and reloaded with a TEG. The fumed

silica insulation is a solid block, which has the same density and placement throughout the tests. To reduce thermal losses from the top face of the copper heater block, a mica ($K = 0.71W/mK$) sheet $75\times75\times0.1mm$ is used. An aperture, the size of TEG module being used is cut through the mica shield so that the module can be placed on the heater block during a test.

4b2: <u>Temperature Measurement and ensuring good thermal contact</u>

As Fig.8 shows, *K*-type thermocouples are placed at various points in the test system to measure the desired temperatures. The thermocouples are connected to a data logger, which is connected to a Laptop computer. The thermocouples used are class 2 tolerance thermocouples, which means they have an accuracy of $\pm2.5℃$. To calibrate the thermocouples, the test system with the thermocouples inserted in it was left at room temperature for two days to ensure that it was in thermal equilibrium with the lab environment. At the start of the week, the data logger was used to record the thermocouple temperatures for 900s with intervals of 15 seconds. The recorded temperature from each thermocouple was averaged. The eight averages were averaged again to get a reference temperature. The offset for each thermocouple was then calculated using Eq.7.

$$OffsetTC = RefTemp - AvrgTCTemp \tag{7}$$

Where $OffsetTC$ (K) is the offset in the thermocouple reading, $RefTemp$ (K) is the calculated reference temperature, and $AvrgTCTemp$ (K) is average temperature recorded by the thermocouple. The calculated offsets were then used to adjust any measurements that were taken using the thermocouples in the system. These thermocouples only need calibration once a year, as recommended by the manufacturer.

The output performance of the TEG module depends on, among other factors, the thermal contact it has with the heat exchanger. A thermal resistance exists between the heat exchanger surface and the TEG. Therefore on hot side, temperature at the TEG surface will be lower than the temperature of the heat exchanger surface. Similarly the temperature on the cold side surface of the TEG will be higher than the temperature of the cold side heat exchanger surface. This would lead to an over all lower ΔT across the TEG compared to the ΔT between the heat exchangers. A good

thermal contact reduces the thermal resistance between heat exchangers and the TEG surface, thereby maximizing the ΔT across the TEG surface. Maximizing the ΔT across the TEG leads to maximizing the electrical power output from the TEG.

Factors such as surface roughness, presence of interstitial materials, surface deformations that take place due to clamping pressure are factors that all affect the thermal interface resistance between the TEG and the heat exchangers. The heat exchangers used in this test apparatus have a surface flatness of $2\mu m$. Polishing and cleaning the surface of the heat exchangers before each test usually removes any dust particles present on it. Graphite pads with a lateral thermal conductivity of $16W/mK$ are used as thermal interface materials to fill any gaps between the TEG and the heat exchangers. The spring coupled stepper motor is used to apply the vendor recommended clamping force on the TEG module being used, to reduce thermal contact resistance between the module and the heat exchangers. The test system uses a load cell to provide feedback of the applied force in order to adjust the stepper motor controller. The test system is capable of maintaining a specified clamping force on the TEG module within $\pm 20N$. This level of precision is considered to be sufficient as a change of $\pm 20N$ in the clamping the force across the TEG for a particular temperature difference across it, has negligible effect (<0.5%) on the output electrical power produced by the TEG, as evident from Fig.10.

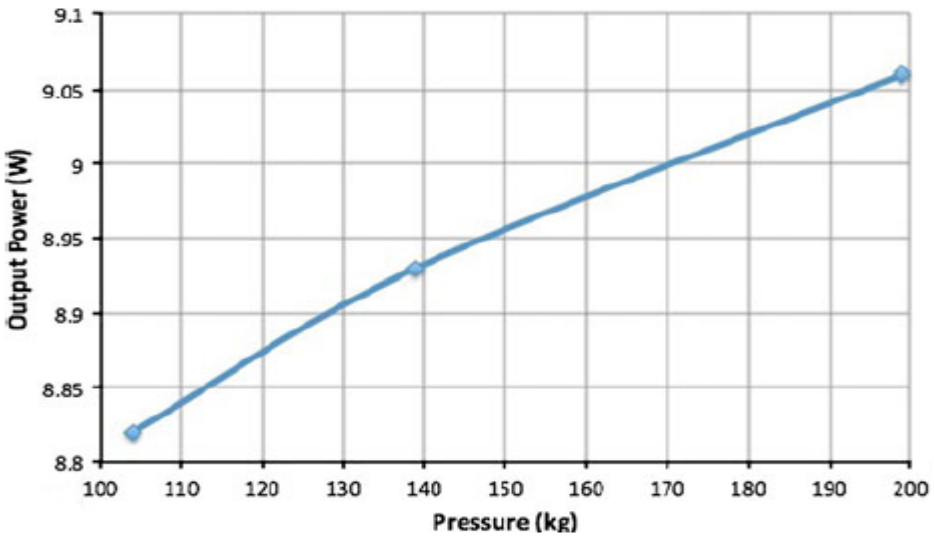

Figure10: Variation of the maximum electrical power produced by a Bi_2Te_3 40mm x 40mm TEG at ΔT=200℃ for different values of clamping pressure [38]

4b.3: <u>Estimation of thermal power losses</u>

An accurate estimate of the thermal losses to ambient from the copper heater block is required to calculate the heat flux flowing through the TEG. To estimate the thermal losses to ambient from the copper heater block the following experiment is conducted.

The thermal steady state temperature of the copper heater block is recorded using thermocouple 6 (T6), as shown in Fig.8, for a fixed value of input electrical power to the cartridge heaters. Thermal steady state for the copper block has been defined as the point when the temperature of the copper block is constant. The temperature of the copper block is considered constant when it has been within $\pm 0.2℃$ for more than 900s.The chiller is turned on and the water temperature is set to 24℃. The copper heater block is moved close to the aluminum heat exchanger so the separation between them is only a couple of *mm*. This is the distance that would normally be between the two heat exchangers if an actual test was running. A TEG module, however, is not placed on the copper heater block and the mica sheet used has no cavity cut through it.

When the copper heater block reaches thermal steady state, it can be said the electrical power input to the cartridge heaters is equal to the thermal power being lost to ambient from the insulated copper heater block. Repeating the experiment for several values of input electrical power, a graph of thermal steady state temperature versus thermal power lost to ambient from the insulated copper heater block can be obtained. Fig.11 shows the results for this experiment. A second order polynomial equation can be used to get an approximate equation for the thermal power lost from the copper heater block in this particular test system to ambient during different values of steady state temperature. As the available modules are rated for a maximum operating temperature of 250℃, data was only collected for steady state temperatures for the copper heater block up to this temperature.

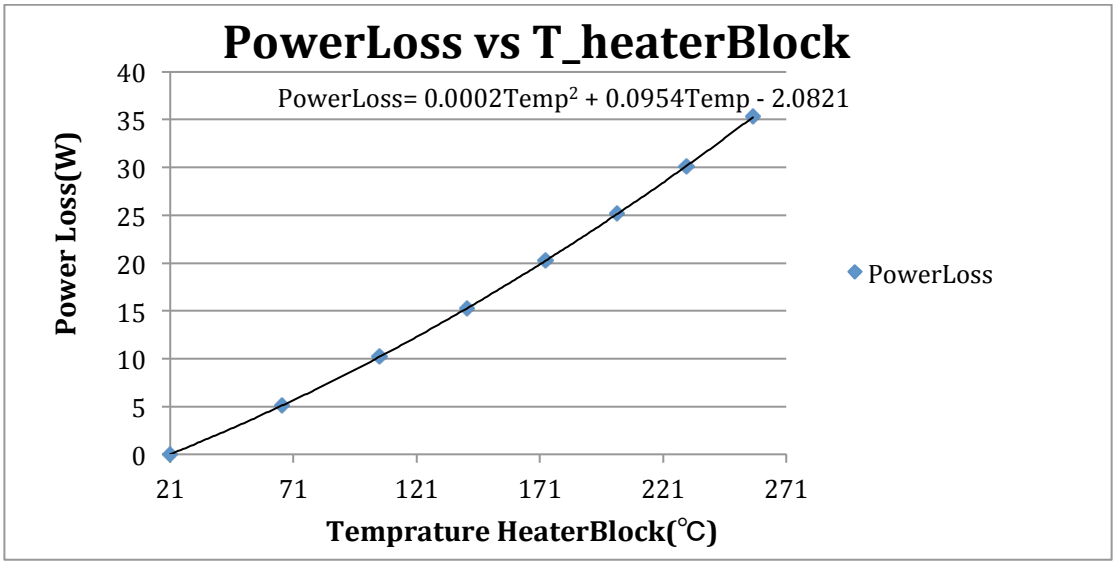

Figure11: Thermal power lost from the insulated copper heater block at different values of copper heater block steady state temperature.

4b.4 Verification of Heat Flux Measurements and Test System Repeatability

Since this test setup will be used to conduct constant heat experiments, the heat flux measurements obtained from it need to be verified. To do this, a reference material, ideally having thermal conductivity and dimensions similar to a typical TEG module that might be encountered in a typical test was used. The reference material should also be able to withstand temperature and pressure that the TEG module might be subjected to. Keeping these parameters in mind, PTFE ("Teflon") was chosen as the reference material to verify the heat flux measurements in the test setup. Teflon has a thermal conductivity of $0.25 W/mK$ and a melting point of 300℃ as specified by the manufacturer. For the purpose of this analysis, a GM250-241-10-12 Bi_2Te_3 TEG module has been used which has a maximum operating temperature of 250℃ and dimensions $40 \times 40 \times 1.2m$. It should be noted that Teflon does becomes softer as it reaches its melting point and this can effect its thickness as well as its contact resistance with the heat exchangers. The contact resistance between Teflon and the heat exchangers changes because as the temperature increases the softening of Teflon results in it filling out the surface deformations on the face of the heat exchangers. This results in a greater contact area between the Teflon and the heat exchangers. To make sure the contact resistance was constant for testing, the sample was repeatedly (3times per sample) heated up to 250℃ and then cooled down to room temperature under constant pressure before the actual testing. It was empirically observed that the change in sample thickness is negligible when testing in the mentioned temperature range.

Three Teflon pieces of the same area ($40\times40mm$) but different thicknesses (*0.5mm, 1mm and 6mm*) were used. Each piece of Teflon was loaded on to the test setup and clamped with the same clamping pressure as would be for a $40\times40mm$ Bi_2Te_3TEG. The clamping pressure for TEGs is specified by the manufacturer and can be converted in to a clamping force value in Newton according to the module size. For the module size being used in this experiment, the required clamping force is 1.92*kN* therefore this is the force with which the Teflon samples are clamped. Each sample is tested for a range of ΔT from $50-150℃$. The chiller water temperature was fixed at $24℃$. The temperature of the copper heater block and the input electrical power to the cartridge heaters for establishing a particular ΔT was recorded after the sample reached thermal steady state. Thermocouples T2 and T5 shown in Fig.8 were used to record the cold side interface and hot side interface temperatures respectively.

Since the temperature readings are taken when the system is in steady state, the hot side interface temperature is assumed to be the copper heater block temperature also. Using the temperature of the copper heater block for steady state, the thermal power lost to ambient was calculated using Fig.11. The heat flux through the Teflon sample is then calculated using Eq.8.

$$Q_h = P_{elec} - Q_{lost} \tag{8}$$

Where $Q_h(W)$ is the heat flux through the Teflon sample from the hot side heat reservoir, $P_{elec}(W)$ is the electrical power supplied to the cartridge heaters and Q_{lost} is the thermal power lost to ambient from the copper heater block. Accounting for the thermal losses, the heat flow through the system can be assumed to be one-dimensional. Using Fourier's Law of heat conduction (Eq.9) the thermal conductivity of the Teflon samples is calculated from the experimental data.

$$Q_h = \frac{kA}{L}\Delta T \tag{9}$$

Where k (W/K) is thermal conductivity, A (m^2) is the effective area and L (m) is effective thickness of the Teflon sample and ΔT is the temperature difference across the sample. Fig.12 and Table1 show the experimentally calculated thermal

conductivity of the three samples used versus the temperature difference across the sample and a comparison with the published thermal conductivity value for the material.

	Sample Thickness (m)	$Q_h\,(W)$	$K\,(W/m.K)$	%age change from original value (0.25)
$\Delta T = 50$℃	0.006	2.90	0.218	-12.8%
	0.001	21.62	0.27	+8%
	0.0005	37.13	0.235	-6%

	Sample Thickness (m)	$Q_h\,(W)$	$K\,(W/m.K)$	%age change from original value (0.25)
$\Delta T = 100$℃	0.006	6.50	0.244	-2.4%
	0.001	43.20	0.27	+8%
	0.0005	75.00	0.234	-6%

	Sample Thickness (m)	$Q_h\,(W)$	$K\,(W/m.K)$	%age change from original value(0.25)
$\Delta T = 150$℃	0.006	8.30	0.208	-16%
	0.001	64.51	0.268	+7.2%
	0.0005	108.89	0.227	+10.8%

Table1: Experimental values of thermal conductivity of Teflon for different thicknesses at $\Delta T = 50$℃, $\Delta T = 100$℃ and $\Delta T = 150$℃and sample area of $0.0016 m^2$

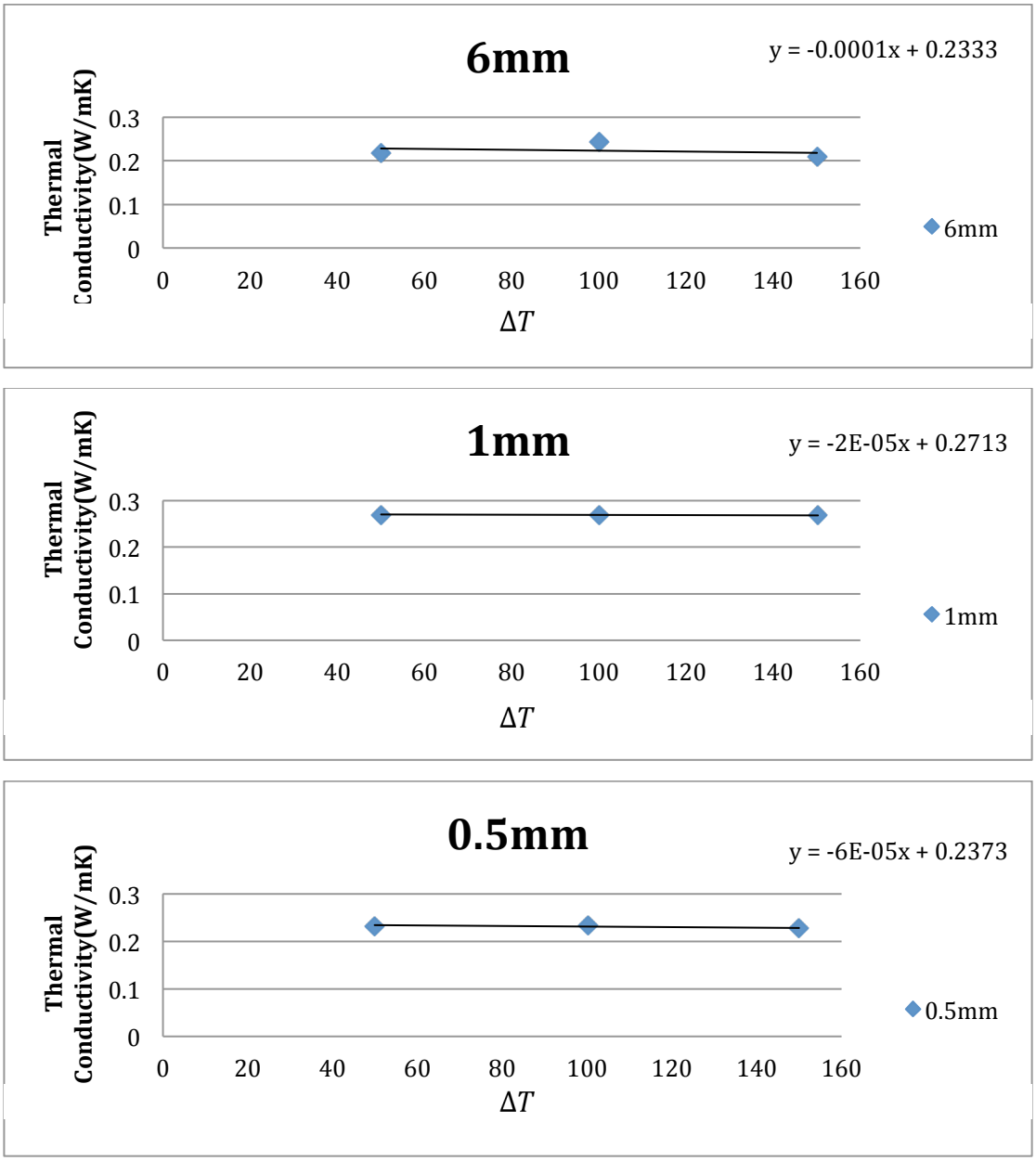

Figure12: Experimental thermal conductivities of the three different samples of Teflon used

It can be seen from Table1 that the values of thermal conductivity for a particular thickness lie within 16% of the value of thermal conductivity specified by the manufacturer ($0.25W/mK$). National Physics Laboratory (NPL) states for laboratories unaccredited by them, a thermal conductivity measurement within 5% of the actual value at ambient temperature is a reliable measurement for insulating materials. The level of uncertainty will be higher with materials of higher conductivity and at higher temperatures. The level of precision NPL refers to has been obtained with the use of guard band heaters and multiple thermocouples placements on the hot and cold heat exchangers. These thermocouples allow the extrapolation of temperature profile of the system all the way to the material interface hence allowing

for precise calculations of heat flux and material thermal conductivity. The present system does not allow for such level of precision.

To confirm the repeatability of the test system, a further experiment was carried out. The Teflon sample with 1mm thickness was used. The Teflon sample is tested for ΔT ranges of $50 - 150℃$. The chiller water temperature was again fixed at $24℃$. The repeatability test is carried out in sets of triplets and the average value of the thermal conductivity of the Teflon sample and the standard deviation of the measured values is calculated. For each ΔT, the Teflon sample is unloaded from the test system, it and the heat exchangers are cleaned with an abrasive pad to remove any remaining parts of the graphite thermal interface pads that may have stuck to the surfaces due to the high temperatures. A new graphite thermal interface pad is placed over the heat exchangers and the Teflon sample is then reloaded into the test system to perform the new test. Fig.13 shows the Teflon thermal conductivity versus ΔT graph.

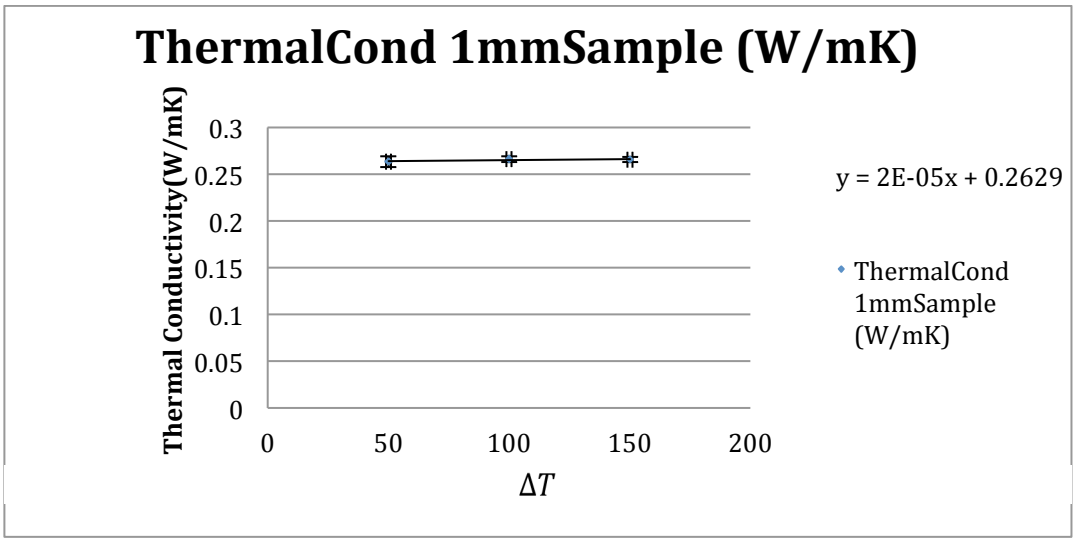

Figure13: Thermal conductivity of Teflon sample 1mm thickness with respect to ΔT with error bars and standard deviation.

The highest standard deviation recorded in the measured values is 2.18%, which is very low. Therefore it can be established that the test system can be used to conduct reproducible tests.

To conclude, using this test system constant heat characterization of TEGs can be performed reliably. The test system allows for temperature measurements with $\pm 0.1℃$ precision, is capable of maintaining a constant clamping force over the TEG modules with $\pm 20N$ can provide up to 1000W of thermal input power to the TEG module and has been compensated for thermal power losses to ambient. The system can be used to test TEG modules of different sizes (up to 62x62mm) and it can also be

used to maintain constant temperatures across the TEG (which will be required for completing the constant heat analysis).

5: RESULTS and DISCUSSION

As discussed in Section 3, in a constant heat system the temperature across the TEG can vary. Consider a TEG sandwiched between two variable temperature heat exchangers. Let Q_h (W) represent the thermal power flowing through the TEG, T_h (K) the hot side exchanger temperature and T_c(K) the cold side exchanger temperature. The thermal conductance ($W/$°C), $K_{variable}$, of the TEG varies according to Eq.10

$$K_{variable} = \frac{Q_h}{\Delta T} \tag{10}$$

Where ΔT=T_h-T_c. The ΔT across the TEG changes with respect to the current drawn from the TEG. Moving from open circuit conditions across the TEG ($I = 0$) to short circuit conditions ($I = I_{sc}$), more heat flux flows through the TEG (because of the increasing Peltier effect). The ΔT across the TEG therefore decreases. For this analysis, it was assumed T_c to be constant. The small variations in T_c affect the average temperature, T_{avrg}, across the TEG only slightly [29]. The electrical conductivity ρ and thermal conductivity k of the TEG vary slightly with T_{avrg}. Therefore, if T_c is fixed, changes in ΔT will be reflected by changes in T_h.

The thermal model of the system can be described as shown in the Fig.14.

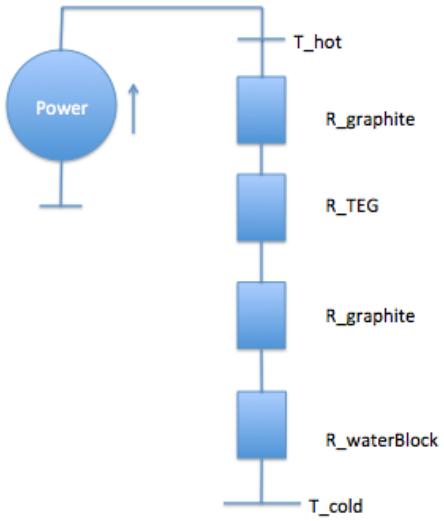

Figure14: Thermal model of the system

In Fig.14, the water block represents the cold side heat exchanger. T_hot represents the hot side face temperature of the graphite covering the TEG. T_cold represents the

cold side heat exchanger temperature. R_graphite, R_TEG and R_waterblock represent the thermal resistances of the graphite sheet, TEG and the water block respectively. 'P' represents the thermal power source to the TEG, in this case being the hot side heat exchanger. The water block has an approximate thermal resistance of $0.1℃/W$. Using the thermal conductance value specified by the manufacturer and using the sheet dimensions the thermal resistance of the graphite sheet can be calculated as follows;

$$R_{graphite} = K_{graphite} \times \frac{A}{L}$$

Where$K_{graphite}$ (W/mK) is the thermal conductance of the graphite sheet used $(16W/m℃)$, A is the effective area of the graphite sheet used and L is the effective thickness of the sheet used. . $R_{graphite}$ is therefore calculated as $0.00496℃/W$. The thermal resistance of the TEG varies according to what the load resistance across the TEG is.

The objective of this experimental investigation was to predict the module thermal steady-state behavior of bismuth telluride (Bi_2Te_3) TEGs *i.e.* predict the position of the maximum power point, the temperature difference established across the module, the open-circuit (V_{oc}) of the TEG for a particular thermal input power to the TEG and the load voltage across the TEG for different values of thermal input power.

Eq.11 gives the thermal power input to the hot junction of the TEG [9,13].

$$Q_h = \frac{kA\Delta T}{L} + \alpha T_h I_{load} - \frac{1}{2} R_{int} I_{load}^2 \qquad (11)$$

Where k (W/mK) is the thermal conductivity, A (m^2) is the effective area and L (m) is effective thickness of the device, α $(\mu V/K)$ is the Seebeck coefficient of the device, I_{load} (A) is the current through the device and R_{int} (Ω) is the internal resistance of the device.

As discussed in the introduction, a TEG operating under constant temperature conditions can be thought of as a constant voltage source with a fixed internal resistance as shown in Fig.15.

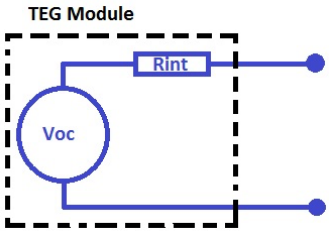

Figure15: Electrical circuit equivalent of a TEG module in constant temperature operation.

Therefore using Eq.12 we can calculate the load voltage across the TEG.

$$V_{load} = V_{oc} - R_{int} I_{load} \tag{12}$$

Where V_{load} (V) is the load voltage across the TEG. The quantities V_{oc} and R_{int} vary with the temperature difference across the TEG and will not be constant in a constant heat system. Therefore for this analysis the values of V_{oc} and R_{int} have been represented by 2nd order polynomial equations derived from experimental characterization of a 40x40mm GM250-241-10-12 Bi_2Te_3 TEG for the desired operating temperature range, shown in Fig.16.

5a: <u>Solving the constant heat equation (Eq.11)</u>

To perform the constant temperature characterization of the sample TEG, a control program was written in Agilent VEE software to apply a constant ΔT across the TEG module. The TEG was loaded in to the test system and clamped with the manufacturer recommended clamping force ($1.9kN$) to ensure good thermal contact with the heat exchangers. The TEG was connected to a DC electronic load, which maintains the TEG in open circuit. Once the desired ΔT was established across the TEG, the program records the value of V_{oc}. The program then tells the electronic load to establish short circuit conditions across the TEG. The TEG is now operating to the right of curve in Fig.5 in Section1. The thermal transport across the TEG increases and therefore a higher heat flux flows through the TEG. The ΔT across the TEG begins to drop immediately. To maintain the same ΔT, the program readjusts the electrical power being supplied to the heaters and iterates until equilibrium is reached. Once the desired ΔT is established, the program records the value of the short circuit current (I_{sc}). Using the V_{oc} and I_{sc} values of the TEG, the VI curve of the TEG was plotted for a particular ΔT. Since it was a constant temperature system, the VI curve of the TEG was expected to be a straight line since the internal resistance of the TEG can be approximated to be constant [9,15,20,38]. The TEG was characterized for a ΔT

range of *25-200*℃, as this is the expected operating ΔT range for the TEG. Fig.16 shows the VI curves obtained from this experiment.

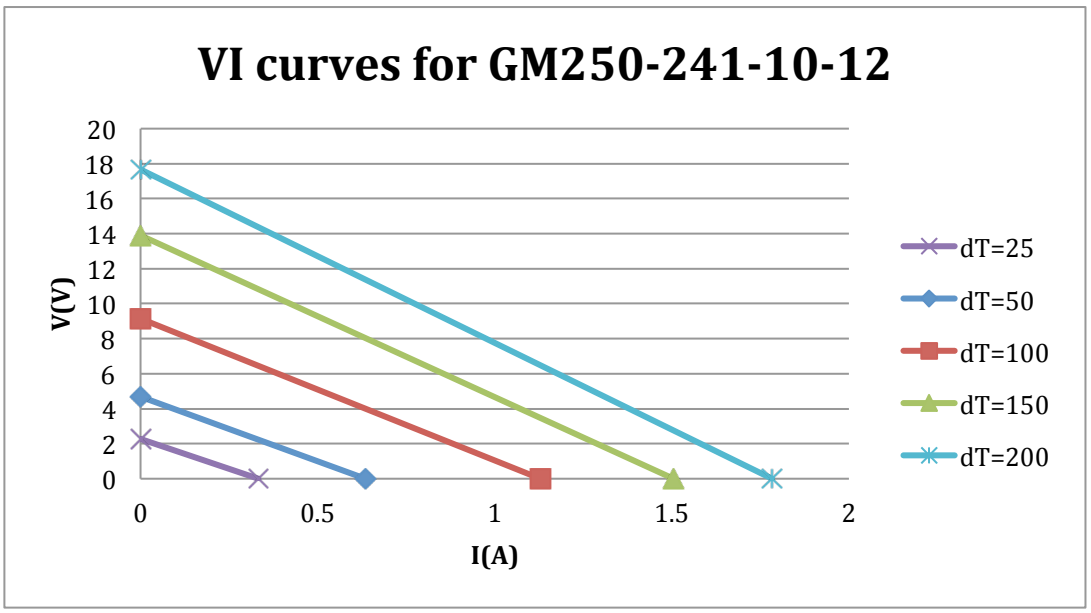

Figure16: VI characterization of GM250-241-10-12 TEG for different values of ΔT

The internal resistance,R_{int}, of the TEG for each ΔT is simply the gradient of the VI curves. The variation of V_{oc} and R_{int} can therefore be observed with respect to ΔT. Fig.17 shows this variation.

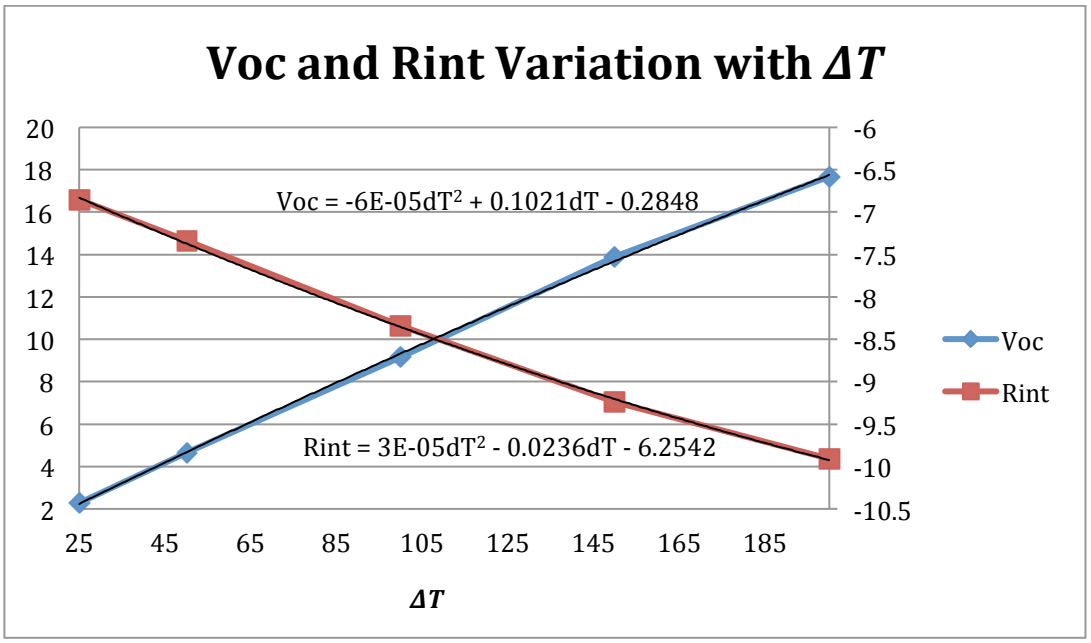

Figure17: Variation of V_{oc} and R_{int} with ΔT for a GM250-241-10-12 TEG

Eq.12 can then be written as Eq.13 [29]

$$V_{load} = u\Delta T^2 + v\Delta T + w - (x\Delta T^2 + y\Delta T + z)I_{load} \quad (13)$$

Using the coefficients from Fig.16 for V_{oc} *(u, v and w)* and R_{int}*(x, y and z)*, V_{load} can be calculated across the TEG for different values of ΔT [26].

Eq.11 can be written as Eq.14 [26] to take in to account the effect of changing temperature on V_{oc} and R_{int}.

$$Q_h = K\Delta T + \frac{u\Delta T^2 + v\Delta T + w}{\Delta T} T_h I_{load} - \frac{x\Delta T^2 + y\Delta T + z}{2} I_{load}^2 \quad (14)$$

Where $K = \frac{kA}{L}$ (W/mK), is the effective thermal conductance of the module.

The thermal conductivity of the TEG also varies with temperature and its variation with respect to ΔT has to also be taken in to account when solving Eq.14. The thermal conductance of the TEG can be calculated using Fourier's Law of heat conduction (Eq.15) and has been experimentally evaluated for the particular TEG being investigated. Fig.18a and Fig.18b show the variation in the effective open circuit and short circuit thermal conductivity of the TEG for the considered operating temperature ranges.

$$Q_h = K\Delta T \quad (15)$$

Where *K* is the effective thermal conductivity of the TEG.

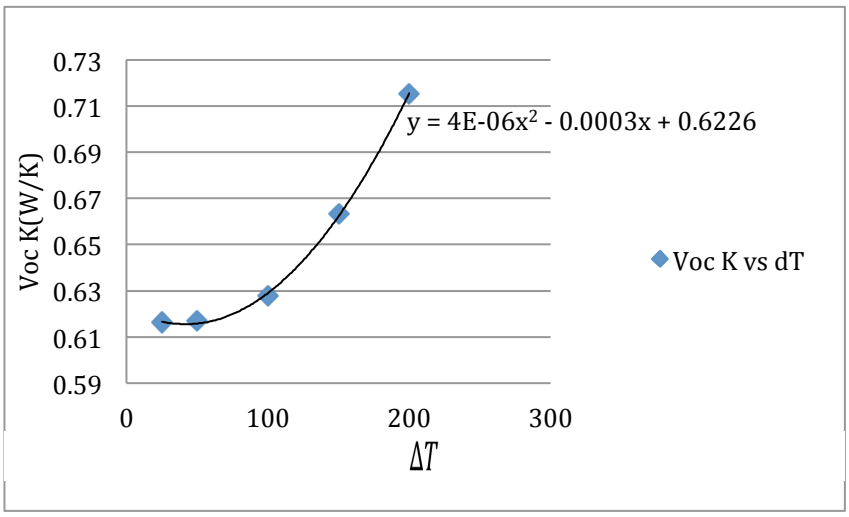

Figure18a: Variation of GM250-241-10-12 40x40mm TEG open-circuit thermal conductance with temperature difference

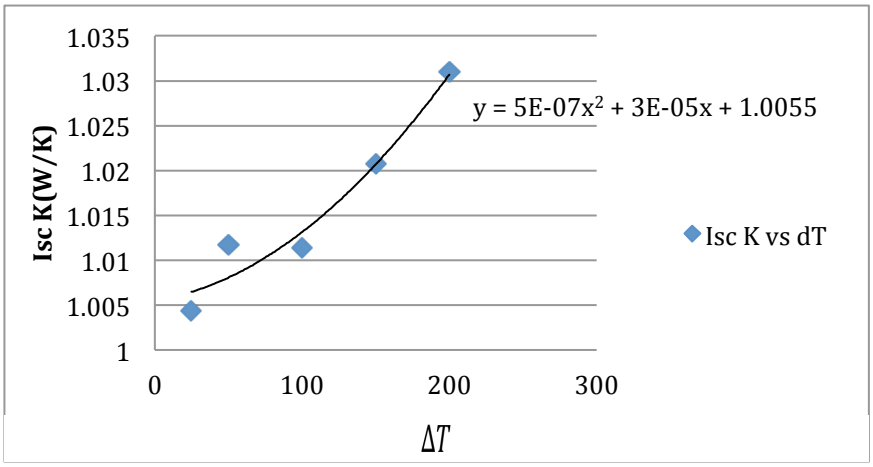

Figure18b: Variation of GM250-241-10-12 40x40mm TEG short-circuit thermal conductance with temperature difference

MATLAB was used to solve Eq.13 and Eq.14 and was used to predict the theoretical TEG behavior for different values of input thermal power. Eq.8 has three possible solutions that MATLAB can calculate. The MATLAB program starts with open-circuit ($I_{load} = 0$) conditions at which point the output electrical power being produced by the TEG is zero and gradually increments the value of I_{load} by a user defined step-size until short-circuit conditions are achieved through the TEG and the output electrical power from the TEG again becomes zero. Moving from open circuit conditions to short circuit conditions, the thermal transport efficiency of the TEG increases and more heat is pumped through the TEG, therefore the temperature difference across the TEG decreases. From the calculation, the ΔT that will be established across the TEG, the load voltages for different values of I_{load} for the TEG and the electrical output power from the TEG can be predicted. For this calculation, the effective open circuit thermal conductivity of the TEG with respect to ΔT is used in calculating the solution. The theoretical maximum power the TEG can produce and theoretical position of the maximum power point can be identified from this calculation. Fig.19 shows the theoretical constant heat characterization graph obtained for a thermal power input of 150W.

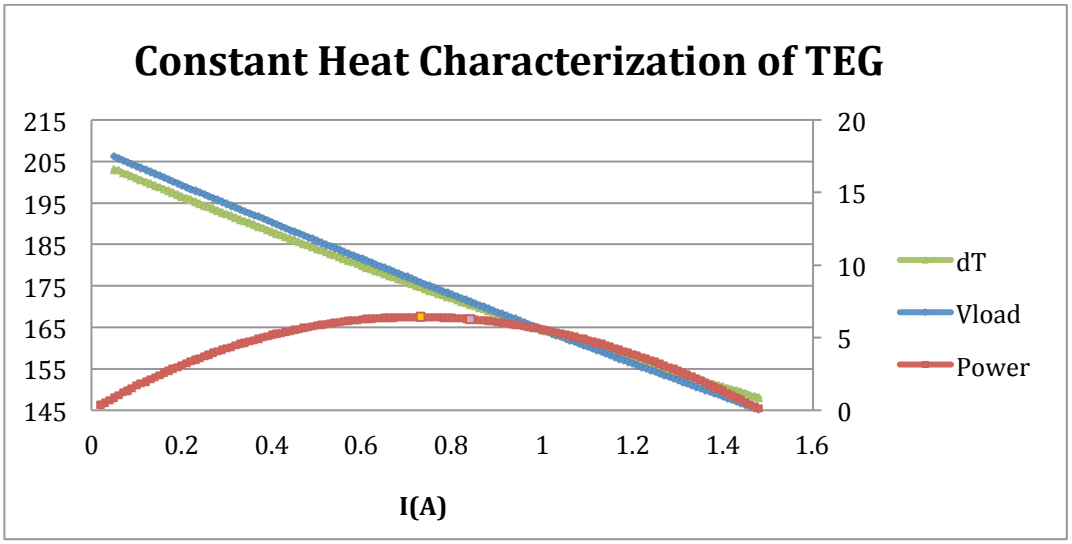

Figure19: Theoretical constant heat characterization of a GM250-241-10-12 TEG using MATALB. The yellow data point on the graph indicates the true maximum power point at $\beta_{max} = 0.567$ and electrical power output of 6.43W. The electrical power output at $\beta = 0.5$ is 6.33W indicated by the purple data point (increase of 1.58%). Input thermal Power=150W.

5b: <u>Experimental Validation</u>

To complete the analysis, experimental validation of the results was required. To experimentally investigate the position of the maximum power point of the TEG the test system described in section 4b was used.

A program is written in Agilent VEE to maintain a constant thermal input power to the TEG. As discussed in Section3, the maximum power point lies to the left of the maximum power point curve in constant heat system. Therefore at the MPP, the value of β will always be greater than or equal to 0.5. The program starts by setting the desired input thermal power and the clamping force for the TEG and then measures the value of V_{oc} using the electronic load once in equilibrium. The program then sets, using the electronic load, V_{load} using the value of β. The value of V_{load} with respect to V_{oc} is updated every ten seconds. The program then waits for the system to reach thermal equilibrium. Thermal equilibrium in this analysis is defined as when the ΔT across the TEG is steady with in $\pm$0.2°C for more than 1800s. This time duration has been empirically determined to be sufficient for thermal equilibrium to be reached.

Once steady state is reached, the program increments the value of β by 0.1 and waits again for the system to reach steady state. The value of β is incremented until the

output electrical power being produced by the TEG decreases and is less than the output electrical power for β_{max} by more than 1%.

The TEG module used to perform this experimental analysis is a GM250-241-10-12 provided by European Thermodynamics (ETL). The manufacturer has specified a maximum working temperature of 250℃ for this TEG for a maximum thermal input power of 180W. However, it should be noted that this maximum input thermal power does not take in to account the thermal power being lost to ambient. Using the data from Fig.11 in Section4, which was used to determine the power loss in the system, the actual maximum thermal power input to the TEG was determined. These TEGs are rated for a maximum operating temperature of 250℃ (above this temperature the solder joining the wires to the TEG melts). It was decided to have a maximum input electrical power to heaters that would lead to a temperature of 245℃. The power loss at this temperature is then calculated using Fig11 from Section4.

The TEG was tested for three different input powers initially. The heater electrical power was set to 180, 140 and 120W. Table2 and Fig.19 show the output electrical power curve for the TEG for these input powers when compensated for with the thermal losses to ambient.

Input Electrical Power (W)	Input Thermal Power to TEG (W)	Output Electrical Power Simulation (W)		Output Electrical Power Experimental (W)		β_{max}		%age increase in O/P electrical power from TEG $\beta_{0.5} \rightarrow \beta_{max}$		ΔT	
		$\beta_{0.5}$	β_{max}	$\beta_{0.5}$	β_{max}	Sim.	Exp.	Sim.	Exp.	Sim.	Exp.
120	102.58	3.68	3.77	3.84	3.96	0.592	0.59	2.4	3.125	126.8	126.3
140	119.54	4.62	4.72	4.82	4.95	0.576	0.59	2.16	2.7	144.7	144.8
180	153.25	6.51	6.61	6.76	6.85	0.562	0.56	1.53	1.33	178.0	178.4

Table2: Comparison of Simulation and Experimental Output electrical power from the TEG for β_{max} and $\beta_{0.5}$ for a given thermal input power to the TEG.

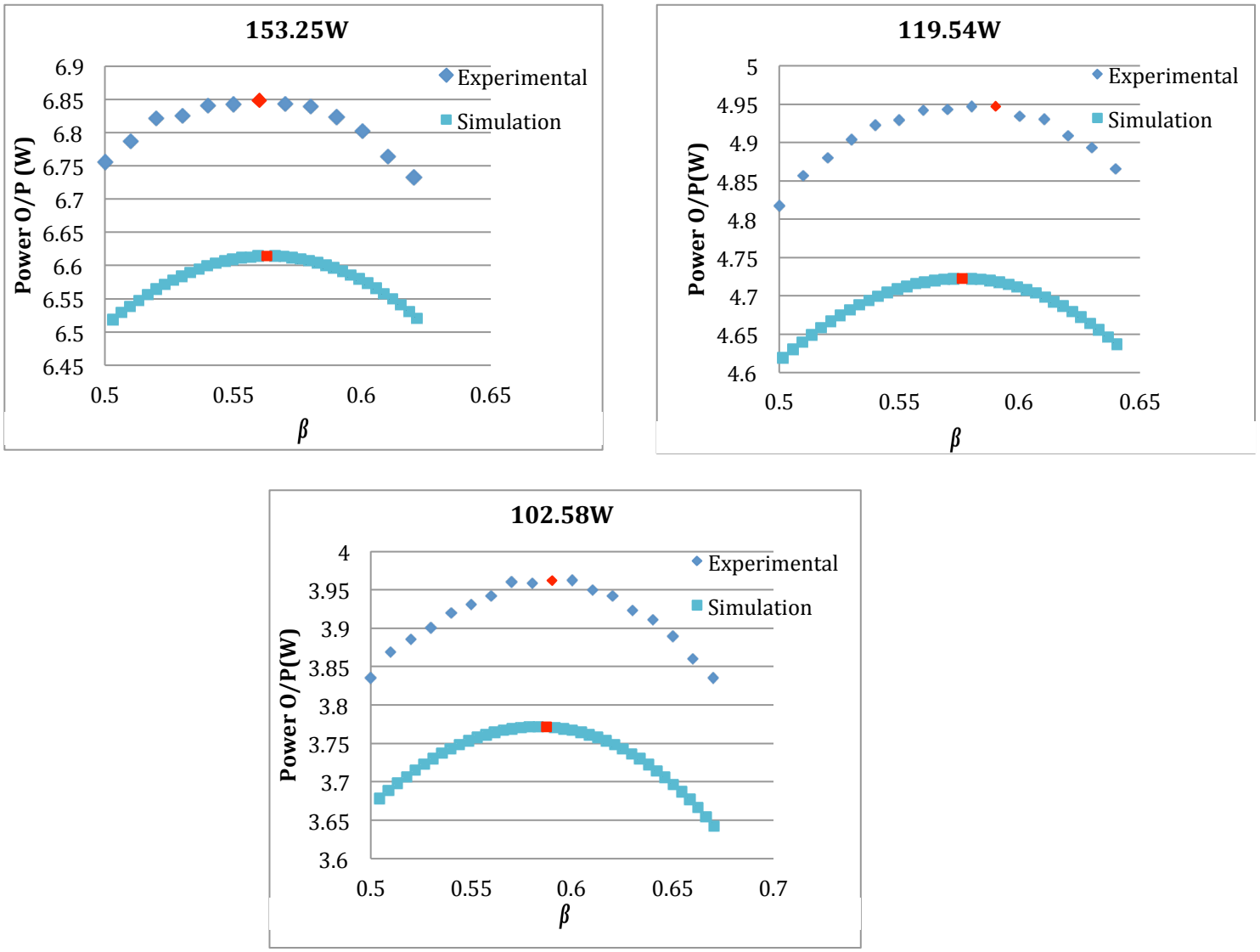

Figure20: TEG electrical power output with respect to β. Red points highlight the position of Maximum Power Point. Comparison of simulation and experimental results

5c: <u>Discussion</u>

From the obtained results we can conclude that for constant heat systems, the maximum power point lies at a value greater than $\frac{V_{oc}}{2}$ ($\beta = 0.5$). It is also observed that as the thermal input power to the system and consequently the ΔT across the TEG increases, the value of β_{max} decreases. β_{max} should have an upper limit as well because moving from open circuit to short circuit conditions, the electrical power output from the TEG falls to zero. How ever this has not been investigated in these experiments.

The thermal to electrical efficiency for TEGs is calculated as

$$\eta = \frac{P_{elec}}{Q_h} \tag{11}$$

Where $P_{elec}(W)$ is output electrical power of the TEG. As pointed out by [29], an increase in P_{elec} will lead to a direct increase in efficiency of the TEG for a given Q_h. This is observed in the MALTAB calculations and experimental results in this analysis also. Table3 shows the increase in TEG output efficiency if the system is operating at the true maximum power point for a GM250-241-10-12 TEG using the experimental values. Though the increase is smaller than that predicted by [26], for systems where large numbers of TEGs are being used together, this could prove beneficial.

Input Thermal Power (W)	Output Electrical Power Experimental (W)		Efficiency (%)	
	$\beta_{0.5}$	β_{max}	$\beta_{0.5}$	β_{max}
102.58	3.84	3.96	3.7	3.9
119.54	4.82	4.95	4	4.1
153.25	6.76	6.85	4.4	4.5

Table3: Comparison of TEG thermal to electrical efficiency using β_{max} and $\beta_{0.5}$

It should be noted that even though the MATLAB calculation uses physical data obtained from the 40x40mm GM250-241-10-12 Bi_2Te_3 TEG, its obtained coefficients for V_{oc} and R_{int} and the effective TEG thermal conductivity can be scaled accordingly to test other Bi_2Te_3 TEGs. The MATLAB calculation can therefore be used to test TEGs with different sizes and different number of pellets.

The next step in this analysis is for the TEGs to be tested for a range of input thermal powers to observe the complete trend of β_{max}. The test also needs to be performed in sets of triplets for each input thermal power to check the repeatability of the behavior exhibited by the TEG. Also a different GM250-241-10-12 Bi_2Te_3 TEG needs to be tested to see how two modules from the same batch would respond to same input thermal power. According to [14] there is a variability of 5-10% in terms of output power produced between two modules with similar physical dimensions.

The current model for the TEG uses a number of simplifications that the experimental results do not take in to account and hence the model accuracy can be improved but only with a lot of added complexity. At the moment, the MATLAB calculations are within 5% of the experimentally observed values. Fully incorporating the variation of the effective thermal conductivity K of the TEG module with respect to β at different values of ΔT rather than just using the open-circuit thermal conductivity K when solving Eq.14, the MATLAB calculations can be further improved to match closely with the experimental data.

This work has aimed to provide further insight into how TEGs operate under constant heat conditions with the aim of complementing the work done by Montecucco *et.al* [26] by providing experimental evidence for the true position of the maximum power point of thermoelectric generators under constant heat conditions.

Future work will involve following through with the suggestions in the last two paragraphs of pg39 and publish the findings in Journal of Electronic Materials, Applied Energy, Applied Thermal Engineering or IEEE Transactions Measurement and Technology.

6. Bibliography

1. Zebarjadi M. Esfarjani K. Dresselhaus M.S. Ren Z.F. and Chen. G. 2011. Perspectives in Thermoelectrics - from fundamentals to device applications. Energy and Environmental Science, pg. 5147-5162.
2. Elsheikh M.H. Shnawah D.A Sabri M.F.M. Said S.B.M Hassan H.M. Bashir M.B.A Mohammad M. 2014. A review on thermoelectric renewable energy: Principle parameters that affect their performance. Renewable and Sustainable Energy Reviews vol30, pg.337-355
3. Karri M.A. Thacher E.F. and Helenbrook B.T. 2010. Exhaust Energy conversion by thermoelectric generator: Two Case Studies. Energy Conversion and Management, vol.52, pg.1596-1611.
4. Zheng X.F, Liu C.X, Yan Y.Y and Wang Q. 2014. A review of Thermoelectrics Research-Recent Developments and potentials for sustainable and renewable energy Renewable and Sustainable Energy Reviews, vol.32, pg.486-503
5. Lofy J, Bell LE. Thermoelectrics for environmental control in automobiles, 2002, Proceedings of the 21st IEEE international conference on thermoelectrics, Long Beach, CA. pg. 471–476
6. Karri M.A. Thacher E.F. and Helenbrook B.T. 2010. Exhaust Energy conversion by thermoelectric generator: Two Case Studies. Energy Conversion and Management, vol.52, pg.1596-1611.
7. Tritt M. T. Subramanian M.A. 2006. Thermoelectric Materials phenomena and applications: A bird's eye view. MRS Bulletin, vol31, pg.188-194.
8. Min G. and Rowe D.M. 1997. Evaluation of Thermoelectric Modules for Power Generation. Journal of Power Sources, vol.73, pg.193-195.
9. Karabetoglu S. Altug S. Fatih O.Z. and Sahin T. 2012. Characterization of a thermoelectric generator at low temperatures. Energy Conversion and Management, vol.62, pg.47-50.
10. Dalola S. Ferrari M. Ferrari V. Guizzetti M. Marioli D. and Taroni A. 2009. Characterization of Thermoelectric Modules for Powering Autonomous Sensors. IEEE Transaction on Instrumentation and Measurement, vol.58, No.1, pg.99-107.
11. Takazawa H. Obara H. Okada Y. Kobayashi K. Onishi T. and Kajikawa T. 2006. Efficiency measurement of thermoelectric modules operating in the

temperature difference of up to 500K. International Conference on Thermoelectrics 2006 Vienna. (ICT 2006), pg.189-192.

12. Rowe D.M. 2006. Thermoelectrics Handbook: Macro to Nano. Boca Raton: Taylor and Francis
13. Snyder G.J. 2009. Thermoelectric energy harvesting. Energy Harvesting Technologies, Springer, pg.325-336
14. Montecucco A. Siviter J. Knox A.R. 2014. The Effect of temperature mismatch on thermoelectric generators electrically connected in series and parallel. Applied Energy, vol.123, pg.47-54.
15. Anatychuk L.I. and Havrylyuk M.V. 2011. Procedure and Equipment for Measuring Parameters of Thermoelectric Generator Modules. Journal of Electronic Materials, vol.40, No.5, pg. 1292-1297
16. Rauscher L. Fujimoto S. Kaibe H.T. Sano S. 2005. Efficiency determination and general characterization of thermoelectric generators using absolute measurement of the heat flow. Measurement Science and Technology, vol.16, pg.1054-1060
17. Ewert MK. Terrestrial and aerospace solar heat pump development: past, present and future. ASME paper at Solar '98, Albuquerque, NM; 1998.
18. Caillat T, Fleurial J, Borshchevsky A. Development of high efficiency thermo-electric generators using advanced thermoelectric materials
19. Tanimura, T. Case study of thermoelectric power generation system utilizing combustion heat of solid waste Proceedings of the 4th Thermal and Electric Energy Symposium, 1998. pg65-81.
20. Rowe D.M. 2006. Thermoelectrics Handbook: Macro to Nano. Boca Raton: Taylor and Francis.
21. Ramadass YK, Chandrakasan AP. 2011. A battery less thermoelectric energy harvesting interface circuit with 35mV startup voltage. IEEE Journal Solid State Circuits 2011. vol41, pg46.
22. Elefsiniotis A, Kokorakis N, Becker T, Schmid U. A thermoelectric based energy-harvesting module with extended operational temperature range for powering autonomous wireless sensors in aircraft 2014. Sensors and Actuators A: Physics vol206, pg159-164.

23. Rosado-Sandoz E. Stevens R.J. 2009. Experimental Characterization of Thermoelectric modules and comparison with theoretical models of power generation. Journal of Electronic Materials, vol.38, No.7, pg.1239-1244
24. Han S.H. Kim H.Y. Kim Y.S. Um S. Hyun M.J. 2010. Performance measurement and analysis of a thermoelectric power generators, 12th IEEE Intersociety conference on Thermal and Thermo-mechanical Phenomena in Electronic Systems, Las Vegas (ITherm), pg.1-7.
25. Carmo J.P. Antunes J. Silva M.F. Riberio J.F. Goncalves L.M. Correria J.H. 2011. Characterization of thermoelectric generators by measuring the load dependence behavior. Measurement, vol.44, pg.2194-2199.
26. Montecucco A, Siviter J, Knox A.R. 2015. Constant heat characterization and geometrical optimization of thermoelectric generators. Applied Energy, pg.248-258, vol.149
27. Y. Apertet, H. Ouerdane, O. Glavatskaya, C. Goupil and P. Lcoeur, Optimal working conditions for thermoelectric generators with realistic thermal coupling. 2012. EPL vol97 28001.
28. Min G. Principle of determining thermoelectric properties based on IV curves. 2014. Measurement Science and Technology vol26
29. Montecucco A. Knox AR. Maximum Power Point Tracking converters based on the open circuit voltage method for thermoelectric generators. IEEE Transactions Power Electronics 2015, pg.828-839 vol30
30. Ewert MK. Terrestrial and aerospace solar heat pump development: past, present and future. ASME paper at Solar '98, Albuquerque, NM; 1998.
31. Caillat T, Fleurial J, Borshchevsky A. Development of high efficiency thermo-electric generators using advanced thermoelectric materials
32. Li W. Paul M. Multiphysics Simulations of a Thermoelectric generator. 2015. The 7th International Conference on Applied Energy. Energy Procedia pg633-638 vol.75.
33. Kumar S. Heister SD, Xu X. Salvador JR. Meisner GP. Thermoelectric generators for automotive waste heat recovery systems. Part I: Numerical modeling and baseline model analysis. Journal of Electronic materials 2013. Pg665-674 vol 72.
34. Niu X. Yu J. Wang S. Experimental study on low temperature waste heat thermoelectric generator 2009. Journal of Power Sources pg621-626 vol188.

35. Mayer P, Ram R. Optimization of heat sink limited thermoelectric generators. 2006. Nanoscale Microscale Thermophysics Engineering. pg.143-155 vol10.
36. Youn N. Lee H. Wee D Gomez M. Reid R. Ohara B. Achieving Maximum Power in Thermoelectric Generation with Simple Power Electronics. 2014. Journal of Electronic Materials. No.6 vol43.
37. Gomez M. Reid R. Ohara B. Lee H. Influence of electrical current variance and thermal resistances on optimum working conditions and geometery for thermoelectric energy harvesting. 2013. Journal of Applied Physics : 0-8
38. Montecucco A. Buckle J. Siviter J. Knox A.R. 2013. A New Test Rig for Accurate Nonparametric Measurement and Characterization of Thermoelectric Generators. Journal of Electronic Materials.